Available online at www.sciencedirect.com
SCIENCE DIRECT®
Journal of Photochemistry and Photobiology A: Chemistry 166 (2004) 45–56
Journal of Photochemistry and Photobiology A:Chemistry
www.elsevier.com/locate/jphotochem

Scanning Maxwell stress microscopy of photo-induced charge separation in A–S–D triad monolayers

Masaru Sakomura [a], Masamichi Fujihira [b,*]

[a] *Department of Material Science, Yokohama National University, Tokiwadai, Hodogaya-ku, Yokohama 240-8501, Japan*
[b] *Department of Biomolecular Engineering, Tokyo Institute of Technology, 4259 Nagatsuta, Midori-ku, Yokohama 226-8501, Japan*

Received 29 October 2003; received in revised form 20 December 2003; accepted 5 April 2004

Abstract

Photo-induced charge separation in mixed Langmuir–Blodgett (LB) films containing oriented A–S–D triads and inert matrix molecules was studied by using scanning Maxwell stress microcopy. A, S, and D stand for electron acceptor, sensitizer, and electron donor moieties of the triad, respectively. The change in surface potentials upon photo-excitation corresponded well with creation and disappearance of photo-induced dipole moments in the LB films due to the photo-induced charge separation in the oriented A–S–D triads followed by charge recombination. The observed lifetime of the separated charges in the LB films, however, was longer by several orders of magnitude than that of isolated A–S–D triads in solution observed by transient absorption spectroscopy. The magnitude of the photo-induced surface potentials, i.e. the content of the separated charges with the longer lifetime decreased drastically with the decrease in the concentration of A–S–D triads in the mixed LB films. Therefore, we concluded that the separated charges with the longer lifetime were created by lateral diffusion of photo-produced anion (electrons) and cation radicals (holes) among neighboring A and D moieties, respectively, in the LB films. We also found that addition of a second donor (D′) monolayer next to a layer of D end moieties of the mixed A–S–D monolayer in multilayered LB films enhanced the photo-induced charge separation with the long lifetime. When light harvesting (H) molecules acting as antenna was mixed with the A–S–D triads in place of the inert matrix molecules, the photo-induced charge separation was observed under irradiation of photons, which were absorbed by the H moieties.

Keywords: Photo-induced charge separation; Scanning Maxwell stress microscopy; Surface potentials; Langmuir–Blodgett films; A–S–D triads

1. Introduction

The highly oriented molecules in thin organic films such as Langmuir–Blodgett (LB) films and self-assembled monolayers (SAM) [1] are essential for some molecular functions. Since the study of the first organic molecular photocells based on dye sensitization with molecules bound covalently on an oxide semiconductor electrode reported in the mid-1970s [2,3], photo-electric conversion using such molecular assemblies and its application to molecular photodiodes [4–17] have been one of the main subjects of our laboratory. In the natural photosynthetic reaction center (Fig. 1), solar energy is first captured by light harvesting antenna pigments, then excited energy harvested by the pigments is funneled to a special pair of the charge separation unit by energy migration and energy transfer, and finally an excited electron–hole pair in the special pair can be separated via electron and hole transfer by electron acceptors and donors located appropriately across the membrane [18,19].

This molecular mechanism of photo-electric conversion has been simulated by using an artificial mixed monolayer consisting of light harvesting H and A–S–D triad amphiphilic molecules (Fig. 2) [5–15]. A, S, and D of the triad stand for electron acceptor, sensitizer, and electron donor moieties, respectively. The sensitizer moiety of the triad can absorb light energy by itself, but also can accept the excited energy of H molecules in the mixed monolayer. The A, S, and D moieties are linked covalently in the triad and expected to be positioned in this order across the monolayer due to an amphiphilic property of the triad. Upon excitation of the S moiety followed by intramolecular electron and hole transfer to the A and D moieties, respectively, the charge can be separated unidirectionally across the monolayer in the same way as in the natural photosynthetic reaction center [18].

The LB technique is suitable for making such highly oriented molecular assemblies. But, detailed structures of LB

* Corresponding author. Tel.: +81 45 924 5784; fax: +81 45 924 5817.
E-mail address: mfujihir@bio.titech.ac.jp (M. Fujihira).

1010-6030/$ – see front matter © 2004 Elsevier B.V. All rights reserved.
doi:10.1016/j.jphotochem.2004.04.026

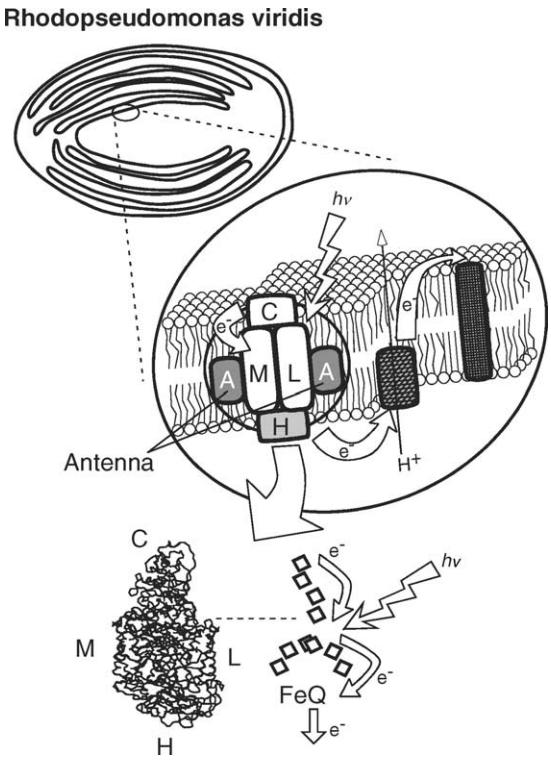

Fig. 1. Schematic representation of the natural photosynthetic reaction center of *Rhodopseudomonas viridis*.

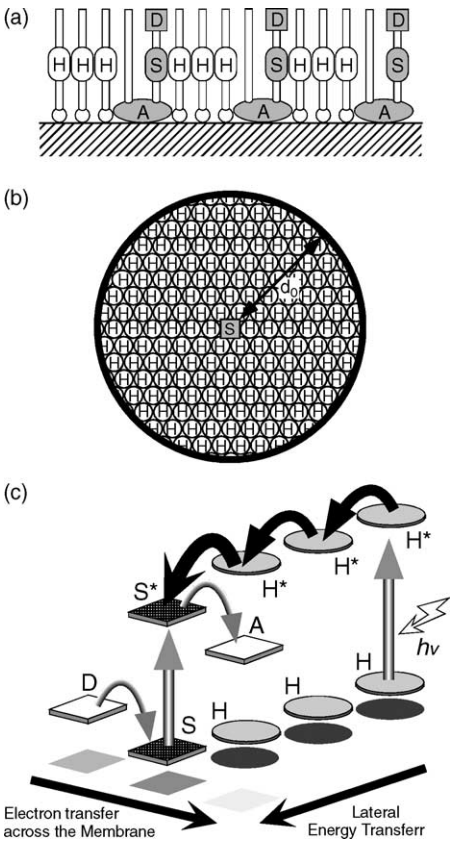

Fig. 2. Schematic representation of (a) a side view, (b) a top view of the artificial photosynthetic reaction center by a monolayer assembly of the A–S–D triad and antenna molecules for light harvesting (H), and (c) energy diagram for photo-electric conversion in the monolayer assembly.

films had not been clarified until these films were studied by scanning probe microscopies (SPMs) [12,15,20–24]. The SPMs, such as scanning tunneling microscopy (STM) [25] and atomic force microscopy (AFM) [26], have been used to analyze surfaces of many levels, from molecular arrangements at interfaces to electronic structures in semiconductors [22]. These SPMs, however, provided only limited information about the chemical nature of systems studied.

In friction force microscopy (FFM) [27–29], the normal and lateral forces are measured simultaneously and separately. In this method, the bending and torsion of cantilever are correlated with the normal and lateral forces exerted by the sample, while the fine resolution of AFM is maintained. Modification of force microscope probe tips by covalent linking [4,13,30–32] of organic monolayers that terminate in well-defined functional groups improves direct probing of molecular interactions and imaging with chemical sensitivity [15,21]. This new chemical force microscopy (CFM) [33–36] has been used to probe adhesion and friction forces between distinct chemical groups [33–40] in organic and aqueous solvents. Knowledge of these forces provides information on processes such as protonation and ionization [36–43].

For the studies of LB monolayer assemblies, information about the orientation of amphiphilic molecules in the monolayers is important, as well as determination of the chemical functionalities. The Kelvin method [44] is a well-established technique for measuring the contact potential differences (CPDs) between a reference electrode and a sample. The CPD for clean metal surfaces is given by the difference in the work functions of the two materials. The work functions can be changed by adsorption of molecules with different dipole moments. The Kelvin method of measuring the CPD makes use of the vibrating capacitor. In the Kelvin method, two conductors are arranged as a parallel plate capacitor with a small spacing. In a simple model, the contact potential between the two materials is $V_{\mathrm{CPD}} = -(\Phi_1 - \Phi_2)/e$, where Φ_1 and Φ_2 are the work functions of the conductors including changes due to the adsorbed layers. A periodic vibration between the two plates at a frequency ω gives an alternating current (ac) with the same frequency ω when the two plates have different work functions.

$$i(t) = (V_{\mathrm{bias}} + V_{\mathrm{CPD}})\omega\Delta C \cos\omega t \quad (1)$$

The technique is to detect the zero point of the ac while the additional bias voltage is applied between the two plates until the electric field between them disappears, thus the CPD can be measured by $V_{\mathrm{CPD}} = -V_{\mathrm{bias}}$ [45]. The Kelvin method has a high sensitivity for the CPD averaged over the whole plate area and does not provide a lateral image of the variation in CPD on the surface on a submicron scale.

The electrostatic force microscopy (EFM) has been used to measure charges [46], dielectric constants [47], the film

thickness of insulating layers [48], photovoltage [49], and electrical potentials [47,50,51]. The spatial resolution of the CPD has been improved using a modified version of the ac scanning force microscope with a Kelvin probe tip, which is called a Kelvin probe force microscope (KFM) [52,53]. The method was further simplified by applying an ac voltage with a frequency of ω being much less than the resonance frequency of the cantilever and by using a resulting Maxwell stress component with a frequency of 2ω as a feedback signal for controlling *z*-piezo [54–58]. The method was named the scanning Maxwell stress microscopy (SMM) [54–58]. We called this new method the scanning surface potential microscopy (SSPM) [59–61].

In order to realize true molecular devices, we have to reduce the size of our LB photodiodes not only in thickness (*z*-direction) but also in the *x*–*y* plane [12,15]. In the previous studies, we described how to fabricate artificial photosynthetic reaction center in nanometer scales by making use of phase separation in mixed monolayers of hydrocarbon (HC) and fluorocarbon (FC) amphiphiles [23,24]. The phase-separated structures were studied by SPMs such as AFM, FFM [22–24], SMM [12,15], and scanning near-field optical/atomic force microscopy (SNOM–AFM) [12,20]. Micro-processing by AFM [12,15] was also applied to fabricate molecular devices in nanometer scales in *x*–*y* plane. We are now undertaking to detect of the photo-induced surface potential change in a single HC island domain of an artificial photosynthetic reaction center embedded in the FC sea by SMM.

In the present paper, we will focus on the detection of charge separation in mixed LB films consisting of A–S–D triad molecules and surfactant HC matrix molecules under laser light illumination with SMM. In the LB films, linear A–S–D triad amphiphilic molecules oriented unidirectionally. By photo-excitation of the S moiety, the electron and hole can be separated unidirectionally. The resulting photo-induced changes in dipole moments of the highly oriented triad molecules will be detected as the surface potential changes of gold electrodes covered with the LB films by SMM. We will also report the effect of addition of the second donor (D′) monolayer in contact with the D end layer of the oriented A–S–D monolayer, i.e. A–S–D/D′ [16], on the photo-induced charge separation. Finally, the charge separation in mixed monolayer consisting of A–S–D triads and light harvesting (H) surfactants upon irradiation of photons absorbed by the H moieties will be described.

2. Principles of the measurement of local surface potentials by SMM

Principles of the local surface potential, i.e. V_{CPD}, measurements using SMM have been described in details, previously [45,60,61]. In the followings, mapping of V_{CPD} between an AFM tip and a metal coated with LB films by SMM will be introduced briefly. The AFM tip should be conductive. Usually a gold-coated tip is used for this purpose, because a work function of gold is well studied and in addition the value of the work function is stable and not changed during the measurement unless the tip is contaminated.

Fig. 3 shows the schematic diagram of SMM (or SSPM) which is based primarily on the design by Yokoyama et al. [54–58]. The electrostatic force on a conducting tip held close to a conducting surface is given by

$$F = -\left(\frac{1}{2}\right) V^2 \left(\frac{\partial C}{\partial z}\right) \tag{2}$$

where V and C denote the Volta potential difference and the capacitance between the conducting surface and the tip, re-

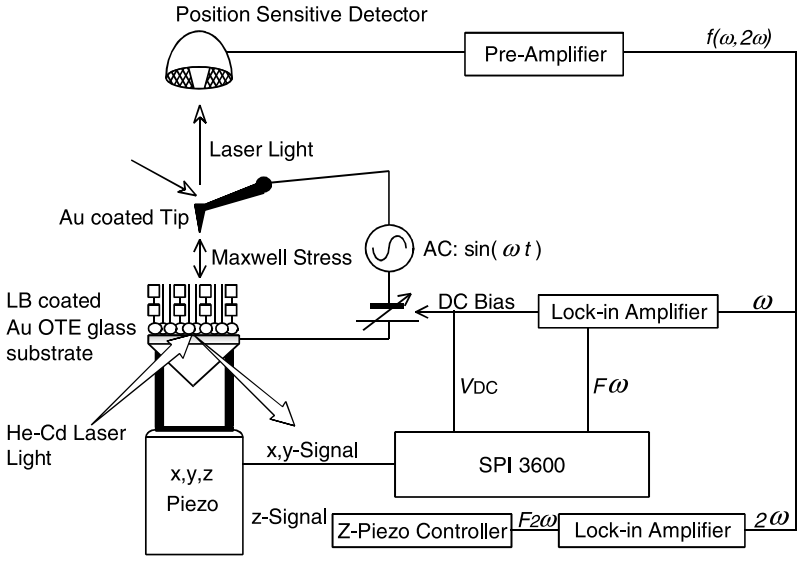

Fig. 3. Schematic diagram of a scanning Maxwell stress microscope.

spectively [60]. If the sample potential against the tip is sinusoidally driven at a frequency ω by an external source without V_{bias}, $V = V_{dc} + V_{ac}\sin(\omega t)$, there appear three force components, i.e. dc, ω- and 2ω-components, each of which gives information on the electrostatic properties of the surface and the surrounding medium. Here, $V_{dc} = V_{CPD}$. If the frequency ω is much less than the resonance frequency of the cantilever, i.e. is off-resonance, the amplitude of vibration of the tip, A, will be given by

$$A = S\left[V_{dc}^2 + 2V_{dc}V_{ac}\sin(\omega t) + \left(\frac{V_{ac}^2}{2}\right)(1 - \cos(2\omega t))\right] \quad (3)$$

where S is the calibration factor relating potential difference to amplitude of vibration and includes the elastic response of the tip (i.e. the spring constant of the cantilever k) as well as $\partial C/\partial z$:

$$S = -\left(\frac{1}{2k}\right)\frac{\partial C}{\partial z} \quad (4)$$

If the 2ω-component is used for the z-piezo controller so as to keep $-S(V_{ac}^2/2)$ constant as shown in the lower pathway of Fig. 3, the amplitude of the ω-component, $2S(V_{dc}V_{ac})$ is linear to V_{dc} (i.e. V_{CPD}) because of constancy of S and V_{ac}. When the amplitude of the ω-component at each measured point on the surface is displayed directly on an x–y frame, the resulting picture is a map of relative values of V_{dc} (i.e. V_{CPD}). Alternatively, if the amplitude of the ω-component is used as a feedback signal for the dc bias so as to compensate the local V_{dc} (i.e. V_{CPD}) (middle pathway of Fig. 3), then the applied V_{bias} is equal to $-V_{dc}$ (i.e. $-V_{CPD}$) and the magnitude, not to the relative value, will be given directly.

3. Fabrication of A–S–D triad monolayer assemblies

How to prepare an LB film is as follows. First, amphiphilic molecules are spread on an aqueous subphase, then compressed by a barrier while monitoring its surface-pressure with an Willhelmy plate, and finally transferred onto a substrate as an LB film.

Before deposition of the LB film, a π–A isotherm, namely a surface-pressure (π) versus area per molecule (A) curve is measured. During the compression, the state of the monolayer is changing from a gas phase, a liquid phase, and finally to a solid phase. When the surface pressure increases beyond a critical value, then the monolayer collapses into a multilayered film. Usually the monolayer in the solid or the liquid phase is transferred onto the substrate.

Fig. 4(a)–(d) illustrate preparation of a Langmuir–Blodgett multilayer film on a hydrophilic substrate. As the hydrophilic substrate for SMM study of LB films, gold semitransparent electrodes (AuOTEs) were used. The hydrophilic substrate is dipped in the subphase when the water surface is clean (Fig. 4(a)). After the spreading and the compression of the monolayer, the monolayer is transferred onto the substrate during withdrawal (Fig. 4(b)). After the monolayer transfer, the surface of the substrate becomes hydrophobic, because long alkyl chains of the amphiphile orient toward the air. As shown in Fig. 4(c) and (d), during the following dipping and withdrawal, two monolayers are transferred with orientations of the amphiphilic molecules shown in Fig. 4(d).

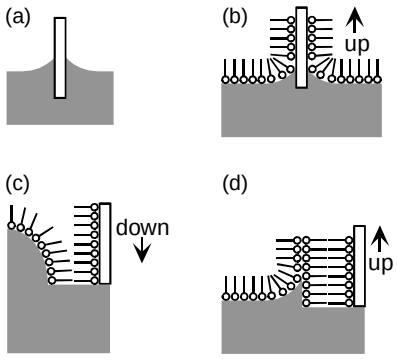

Fig. 4. Preparation of a Langmuir–Blodgett multilayer film on a hydrophilic substrate.

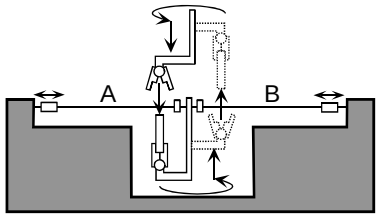

Fig. 5. Schematic diagram of a side view of a monolayer trough for alternate deposition.

LB films with the A–S–D triad for charge separation measurements were deposited by a San-esu Keisoku alternate deposition system. The water surface in a trough of this system is separated by two fixed barriers into three compartments. Two different monolayers can be formed in the two compartments A and B (Fig. 5). Another compartment sandwiched by the two fixed barriers on center of the trough, is usually a pure water surface. The lifter clutching the substrate consists of an upper arm and a lower arm. These arms can move up and down independently and rotate. The under arm can transport a substrate dipped thoroughly into a subphase between A and B compartments without taking it out from the subphase.

4. Detection of photo-induced charge separation in monolayer assemblies

4.1. SSPM of alternate LB films containing unidirectionally oriented A–S–D triads

In the LB films, linear A–S–D triad amphiphilic molecules oriented unidirectionally in two ways with the D tail of the triad towards the air (type-a) or towards the substrate

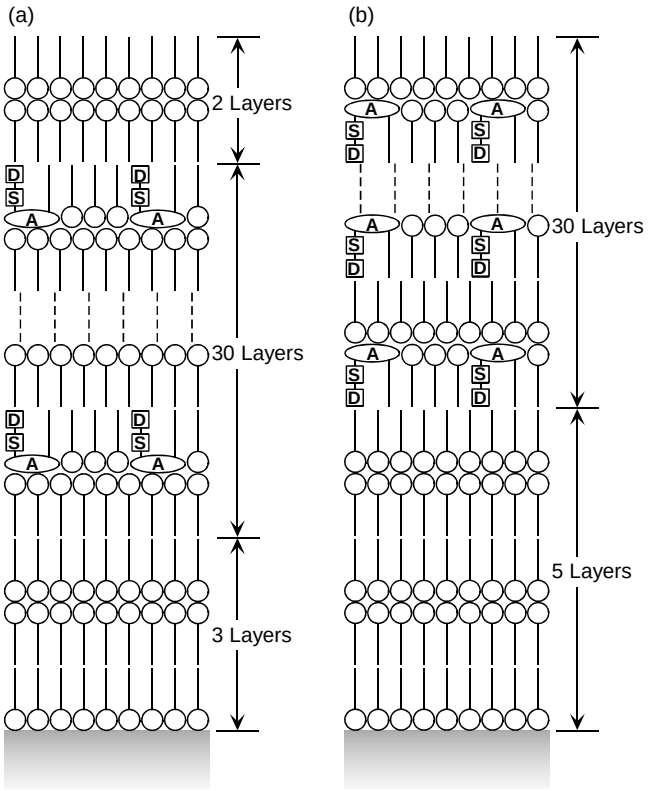

Fig. 6. Unidirectionally oriented A–S–D triads in LB films containing 15 alternate bilayers consisting of a triad–T (1:5) and pure T monolayer. In type-a (a), the D tails of A–S–D triads orient toward the air, whereas in type-b (b) the tails orient toward the substrate.

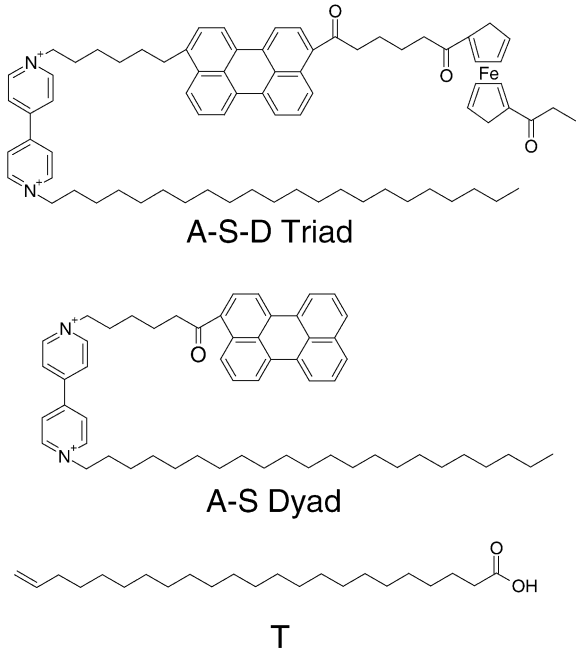

Scheme 1.

plate (type-b) as shown in Fig. 6(a) and (b), respectively. For the fabrication of these LB assemblies, the A–S–D triad and 22-tricosenoic acid (T) shown in Scheme 1 were used. The electron acceptor (viologen, A), the sensitizer (acylated perylene, S), and the electron donor (diacylated ferrocene, D) moieties are expected to be located in this order or reversed order across each alternate monolayer in the LB films. By photo-excitation of the S moiety, the electron and hole can be separated unidirectionally, but with opposite directions in the LB films as in the same way as the primary process in photosynthesis (Fig. 1) [13,15,62]. The resulting photo-induced changes in dipole moments of the highly oriented triad molecules were detected as the surface potential changes of gold electrodes covered with the LB films by SMM under illumination as shown in Fig. 7.

The change in surface potentials of the LB films of types a and b (Fig. 6) under step illumination with He–Cd laser light of 441.6 nm was measured by SMM with a gold coated Si_3N_4 tip and the results are shown in Fig. 8 together with that of a blank LB film. As shown in Fig. 8(a) and (b), the increase in absolute values of the change in surface potentials were observed continuously during illumination for ca. 2 s on the LB films containing the A–S–D triads in type-a and type-b, respectively, but the created surface potentials decayed almost exponentially to the original surface potentials within several ten seconds. The potentials created varied from place to place even on the same sample, but the direction (i.e. the sign) was always the same. Namely, on type-a was observed a positive change in the surface potential corresponding to the increase in dipole moments in the triads whose positive ends were directed towards the air, while the opposite surface potential change was observed on type-b. On the blank LB film, much smaller changes varying from place to place were observed (Fig. 8(c)), but almost always the shift was positive in the same direction as that for type-a.

The gradual changes during the illumination correspond to the increase in the number of the charge separated species, while the exponential decays after shutting the illumination down reflect the decrease in the number of the

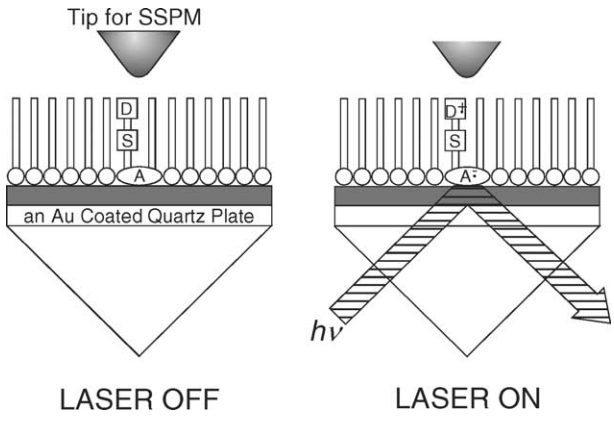

Fig. 7. Detection by SMM of the change in photo-induced surface dipole moments in highly oriented A–S–D triads in artificial photosynthetic reaction centers as the local surface potential changes.

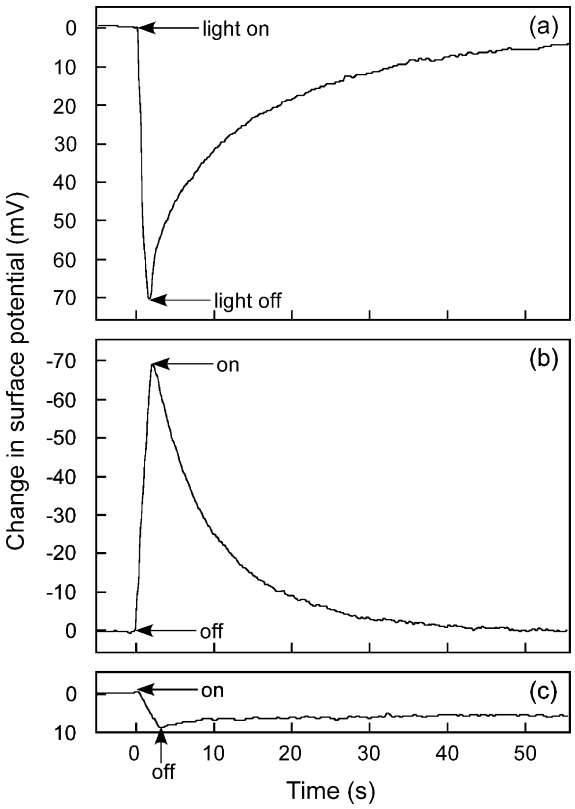

Fig. 8. The change in the surface potential by step illumination for ca. 2–3 s with a He–Cd laser of 441.6 nm wavelength in a total reflection mode on (a) a type-a alternate, (b) a type-b alternate LB film containing 15 unidirectionally oriented A–S–D triad monolayers (shown in Fig. 6), and (c) a blank LB film.

separated charges by recombination. If the charge separation and recombination proceed only within the triads, i.e. via intramolecular processes, it seems that the observed recombination rates were too slow in comparison with the intramolecular recombination rates for an A–S–D triad (Scheme 2) in benzonitrile solutions, as determined by nano- and femto-second transient absorption spectroscopies (Fig. 9) [63]. The stretched molecular conformations in LB assemblies are expected to contribute to prolonged lifetimes of separated charges, however, the difference in decay time between ca. 10 s and 50 ns is too large.

Therefore, the much slower recombination can be interpreted as arising from farther charge separation via a lateral diffusion mechanism of photo-created anion and cation radicals, as illustrated in Fig. 10.

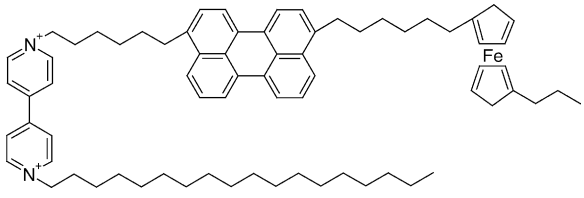

Scheme 2.

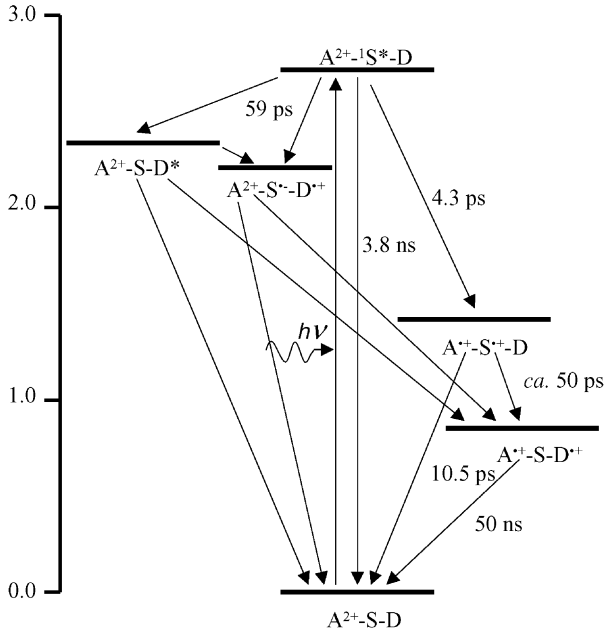

Fig. 9. Summary of kinetics for A–S–D triad (Scheme 2) in benzonitrile.

To confirm the long-lived charge separation by the lateral diffusion mechanism, we also measured the surface potential change on alternate LB films containing A–S dyads (Scheme 1) similar to types a and b. To increase signal intensities, both types of LB films contained 30 bilayers of the alternate monolayers. As shown in Fig. 11(a) and (b), it is clear from comparison with the change observed on a corresponding blank (Fig. 11(c)) that, even on the LB films of unidirectionally oriented A–S dyads, the photo-induced surface potential changes were clearly observed with signs expected from the orientations. Because the intramolecular recombination of the dyad can be expected to proceed on a pico-second time scale (Fig. 9), the observed change in the surface potentials and the slow decays are again rationalized in terms of the same lateral charge separation mechanism, as shown in Fig. 10.

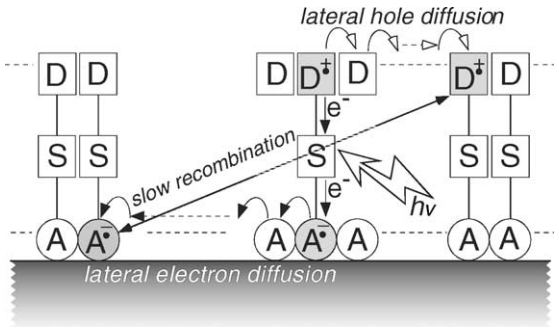

Fig. 10. Schematic illustration of slow charge recombination via lateral diffusion of electrons and holes in the A and the D layer, respectively, in the A–S–D triad monolayer. Anion and cation radicals on the A and the D moieties were created by photo-excitation of the S moieties followed by charge separation.

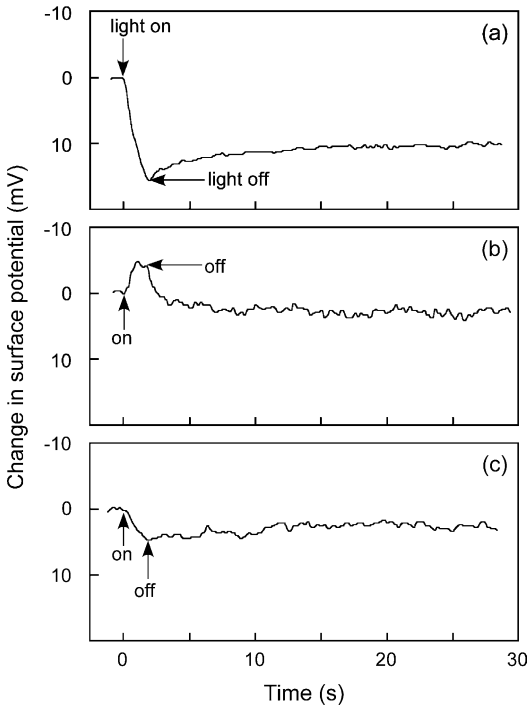

Fig. 11. The change in the surface potential by step illumination for ca. 2 s with a He–Cd laser of 441.6 nm in a total reflection mode on (a) a type-a alternate, (b) a type-b alternate LB film containing 30 unidirectionally oriented A–S dyad (Scheme 1) monolayers, and (c) a corresponding blank LB film.

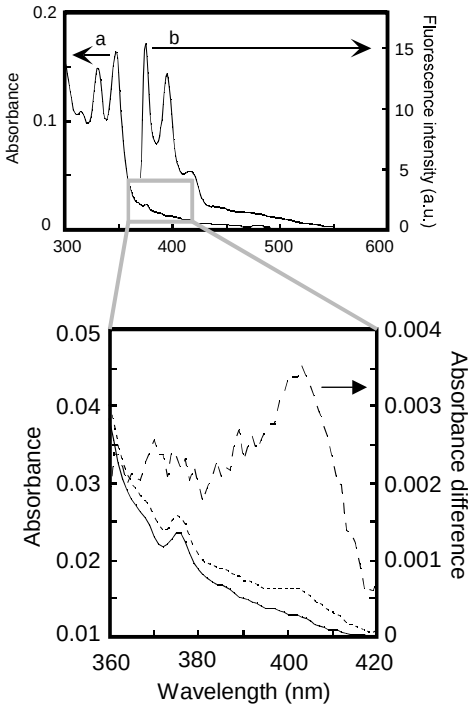

Fig. 12. (a) UV–vis absorption spectra of the mixed LB films of A–S C16 (Scheme 3)–arachidic acid (AA) (molar ratio 1:10, 122 layers). Absorption spectra measured after 5 min UV irradiation at 350 nm (dotted curve) and an absorption difference spectrum (dashed curve) between the two curves, i.e. dotted and solid, are shown in the bottom figure. (b) A fluorescence spectrum of the mixed LB film of A–S C16–AA (81 layers).

4.2. Accumulation of viologen cation radicals in A–S dyad LB films

The long-lived charge separation by the lateral diffusion mechanism assumed from SMM results was also supported by UV–vis absorption and fluorescence studies as shown in Fig. 12. Fig. 12(a) shows two slightly difference absorption spectra of an LB film containing an A–S dyad (A–S C16, Scheme 3) measured under N_2 before (a solid line in magnified spectra shown in the bottom) and after (a dotted line in the bottom) 5 min UV (350 nm) irradiation under N_2. The dashed line in the bottom illustrates an absorbance difference spectrum between the two absorption spectra. It is clear from comparison of the absorption difference spectrum with the spectrum of a methyl viologen cation radical solution produced electrochemically [64] that viologen cation radicals accumulated in the LB film during UV irradiation under N_2. The accumulation of viologen cation radical can be explained by the same mechanism of the lateral charge diffusions.

A fluorescence band of the pyrene moiety (Fig. 12(b)) around 400 nm well overlaps with the absorption band of viologen cation radicals. These results suggest that the photo-produced viologen cation radicals can act as the energy transfer quencher for the excited pyrene moieties (Fig. 13). Fig. 14 shows the considerable decrease of fluorescence intensities with elapsed time of UV irradiation

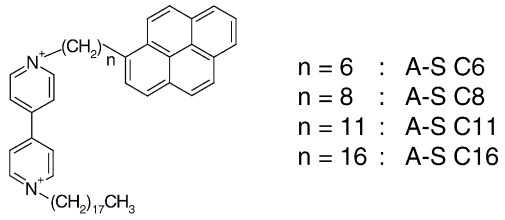

Scheme 3.

under N_2 observed on LB films consisting of one of the A–S dyads (Scheme 3). But, recoveries of the fluorescence intensities were immediately observed upon exposure of the A–S LB films to air after the UV irradiation. The recovering of the fluorescence intensities can be explained due

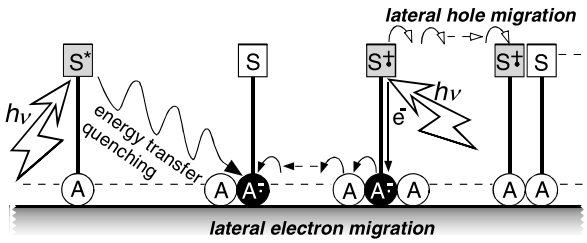

Fig. 13. Schematic illustration of the energy transfer quenching by long-lived viologen cation radicals formed via the lateral charge diffusion.

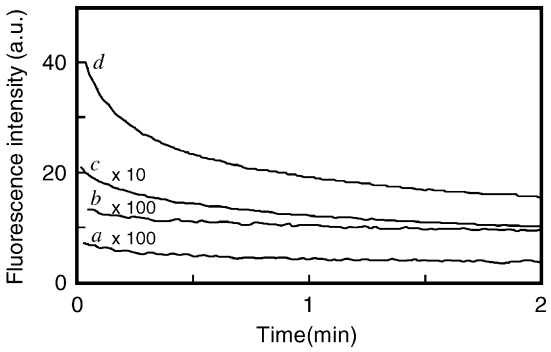

Fig. 14. The changes in the fluorescence intensities of LB films consisting of one of the A–S dyads, A–S C6 (curve a), A–S C8 (curve b), A–S C11 (curve c), and A–S C16 (curve d), and AA (molar ratio, 1:10) as functions of elapsed time. The intensities of the curves a and b and that of the curve c are magnified by a factor of 100 and 10, respectively.

to reoxidization of the viologen cation radicals to viologen dications caused by oxygen in air [65].

In previous studies [66,67], the fluorescence intensities measured before the accumulation of viologen cation radicals estimated by extrapolation of the stationary fluorescence intensity–time curves in Fig. 14 were used to determine the distance dependence of the rate of the electron transfer from excited S to A. Not only viologen but also many other compounds which act as electron acceptors or donors can be changed into energy acceptors owing to photo-chromism via photo-induced electron transfer. The accumulation of the photo-chromic energy acceptor should be taken into account especially when the fluorescence lifetime measurement is employed to study electron transfer kinetics in highly concentrated systems such as LB films and self-assembled monolayers, because averaging of high-speed repetitive measurements is ordinary used for attaining a high S/N ratio.

4.3. *Effect of dilution of A–S–D triad molecules in LB assemblies*

In this section, we examine the effect of dilution of the A–S–D triad molecule embedded in the LB assemblies with an electrochemically inert surfactant. When each molecule of the A–S–D triad is isolated in such a diluted monolayer, the lateral process of the charge diffusion should be inhibited.

The surface potential changes under 125 ms step-functional irradiation of the He–Cd laser beam are shown in Fig. 15(a) and (b) with the schematic representations of the corresponding film structures. The photo-response of the change in surface potentials was observed clearly on the LB assembly containing the high concentration of A–S–D mixed with T (Scheme 1) with the molar ratio of A–S–D:T = 1:5 as shown in Fig. 15(a). On the other hand, the photo-response could not be observed entirely on the LB assembly containing the low concentration of A–S–D mixed with T with

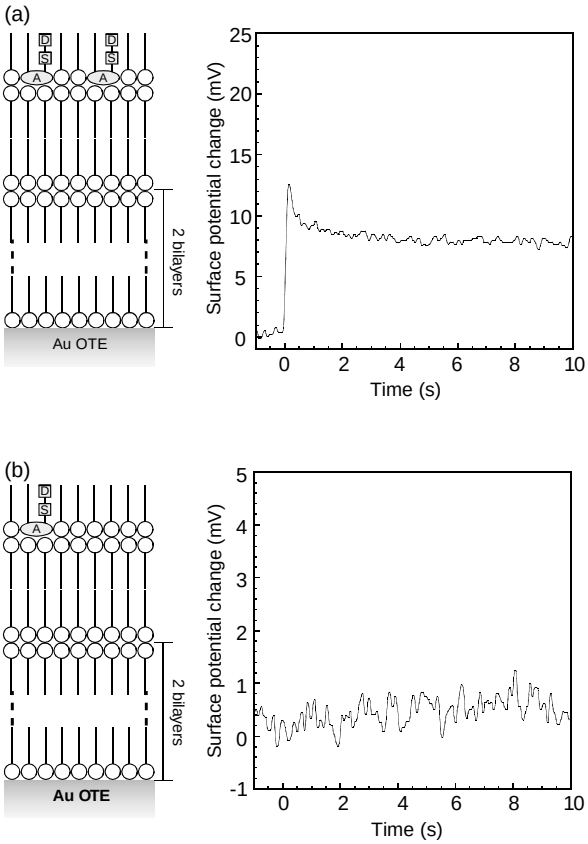

Fig. 15. Photo-induced surface potential change under step illumination by He–Cd laser (441.6 nm) and the schematic representation of the corresponding LB assemblies. After the deposition of the five monolayers of T, a bilayer of T/A–S–D was deposited: (a) T/A–S–D (A–S–D:T = 1:5); (b) T/A–S–D (A–S–D:T = 1:30).

the molar ratio of A–S–D:T = 1:30 (Fig. 15(b)). If the photo-response is proportional only to the light absorption by the S moiety, the observed response will be proportional to the surface concentration of the S moiety. If it is the case, the response will be ca. 1/4. Here, difference in the size of the head groups between A–S–D (ca. 0.6 nm^2 per molecule [5]) and T (ca. 0.2 nm^2 per molecule [1]) is taken into account. Namely, $0.6/(0.6 + 0.2 \times 30)$ divided by $0.6/(0.6 + 0.2 \times 5)$ gives ca. 1/4. The observed photo-response shown in Fig. 15(b) was much less than this expectation. This indicates that the lateral charge migration among A–S–D molecules would be suppressed drastically by the increase in the migration distance as a result of further dilution of the A–S–D monolayer with T. In the closely packed molecular arrangements in LB monolayers formed under high surface pressures, five molecules of T could not thoroughly surround one A–S–D molecule on average, whereas 30 molecules of T could separate A–S–D each other. The average migration rate of A–S–D:T = 1:30 will decrease drastically compared with that of A–S–D:T = 1:5, if the charge migration rate decreases exponentially with distance. This can be rationalized by the distance dependence of electron (or hole) transfer [14].

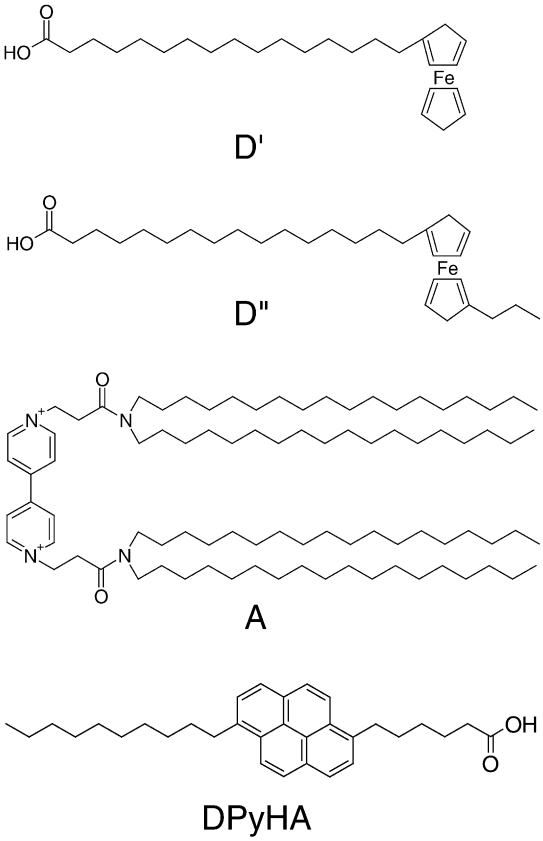

Scheme 4.

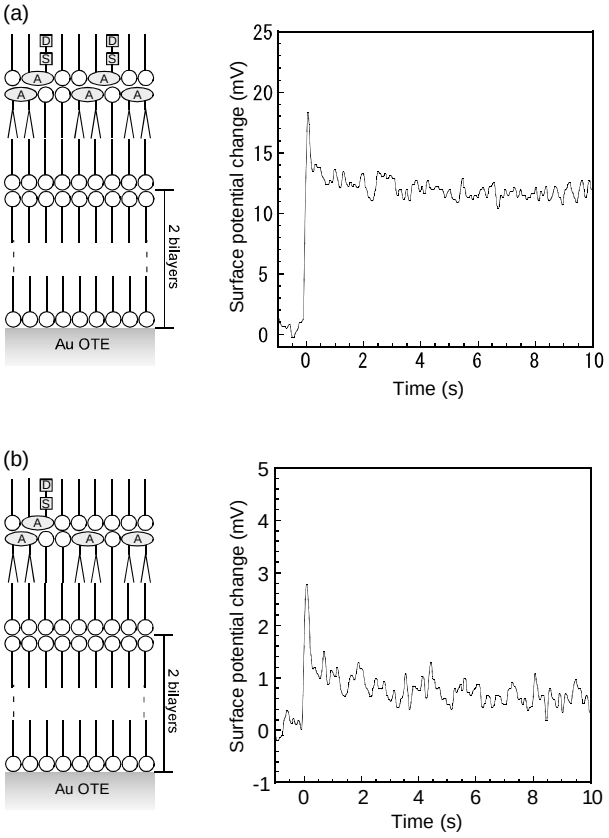

Fig. 16. Photo-induced surface potential change under step illumination by He–Cd laser (441.6 nm) and the schematic representation of the corresponding LB assemblies. After the deposition of the five monolayers of T, a bilayer of A/A–S–D was deposited: (a) A/A–S–D (A–S–D:T = 1:5); (b) A/A–S–D (A–S–D:T = 1:30).

5. Efforts to increase the efficiency of photo-electric conversion by LB assemblies

5.1. Effect of addition of an electron diffusion layer

Next, we examine the effect of addition of an amphiphilic acceptor (A in Scheme 4) layer to the LB monolayers with the same ratios of A–S–D and T as those of Fig. 15. The A layer deposited alternately in the order of A/A–S–D was formed as the mixed monolayer with T with the molar mixing ratio A:T = 1:2 to compensate charges on the hydrophilic head groups, i.e. viologen^{2+} and –COO^{-}. The surface potential changes and the schematic representations of the film structures are shown in Fig. 16(a) and (b). From comparison between Fig. 15(a) and Fig. 16(a), addition of the A layer to the A–S–D layer (A–S–D:T = 1:5) increased the photo-signal but the change was not significant. In the mixed A–S–D monolayer with T in the molar ratio of A–S–D:T = 1:5, the surface concentration of A–S–D molecule is so high that the separated charges easily migrate between adjacent A–S–D molecules. In the condition of the high concentration of A–S–D in the A–S–D layer, the addition of the A layer, which is suppose to enhance migration of separated charges, was not significantly effective.

The effect of addition of the A layer was, however, significantly observed in combination with the diluted A–S–D layer (A–S–D:T = 1:30). As described above, if we assume that the photo-response is proportional only to the surface concentration of the S moiety, the photo-response in Fig. 16(b) will be ca. 1/4 of that in Fig. 16(a). Although the observed result in Fig. 16(b) was smaller than this expectation, the photo-response was clearly observed with the A/A–S–D structure in contrast with the response shown in Fig. 15(b). This result supports that the A layer has the capability to enhance electron migration and electron accumulation. In other words, the A layer plays a role of an electron pool in our artificial photosynthesis system in the same way as quinone pool in natural photosynthesis.

5.2. Effect of addition of a second donor bilayer

The A compound includes the same acceptor moiety as the A–S–D triad, i.e. viologen moiety, therefore vectorial electron transfer between A–S–D and A would not occur in the LB assemblies of A/A–S–D structure since there is no driving free energy for the further electron transfer, $\Delta G = 0$. To increase the charge separation efficiency, the increase in the lifetime of the charge separation perpendicular to the film by adding a second donor D′ or an acceptor A′ to

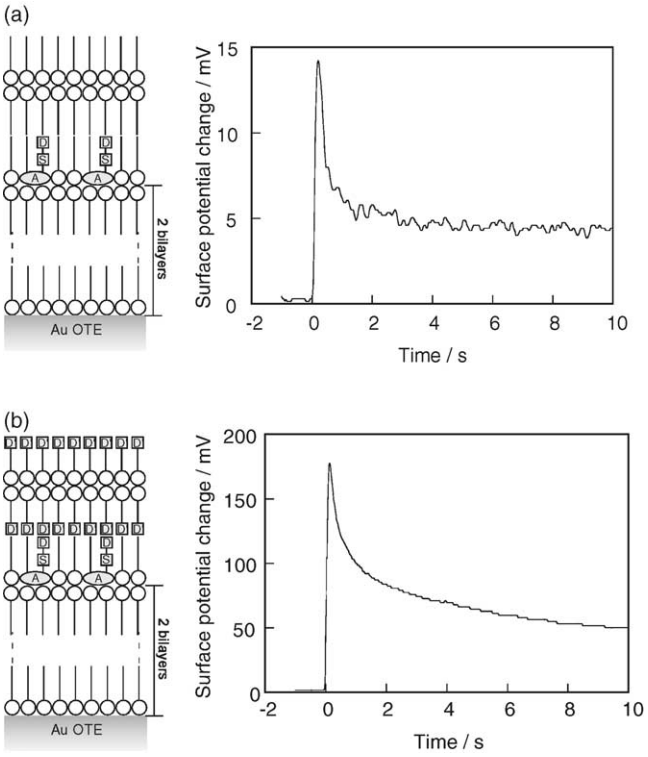

Fig. 17. Photo-induced surface potential change under step illumination by He–Cd laser (441.6 nm) for the LB assemblies (a) without and (b) with a pure D′ bilayer. The A–S–D mixed monolayer consists of A–S–D and T (1:5).

form A–S–D–D′ or A′–A–S–D quadruplet should be examined. In fact, in the reaction center of natural photosynthesis, A′–A–S–D structure is used for its efficient charge separation [68]. Because of laboriousness of quadruplet syntheses, the quadruplet structure by depositing a D′ monolayer (Scheme 4) on a D end of an A–S–D monolayer (Scheme 1) is constructed in this section. The ionization potential of the donor moiety in D′ molecule is smaller than that of the D moiety of the A–S–D triad, therefore the layer can act as a second donor layer with a sufficient driving free energy.

Fig. 17(a) shows the surface potential change of the reference A–S–D monolayer film under step illumination for 125 ms with a He–Cd laser and the schematic representation of the structure of the corresponding LB assembly. The LB multilayer consists of pure T monolayers and a mixed A–S–D monolayer with T in a molar mixing ratio of 1:5 alternately deposited on an AuOTE. The surface potential change and the schematic representation of the structure for the LB multilayer with a pure bilayer of D′ is shown in Fig. 17(b). It is remarkable that the photo-induced surface potential change increased about one order of magnitude over that of the reference A–S–D film by the addition of the D′ bilayer. The drastic increase in the surface potential by the addition of the D′ is attributable to the efficient lateral diffusion due to the prolonged lifetime of the perpendicular charge separation by the A–S–D/D′ quadruplet system.

5.3. Simulation of primary process in photosynthetic reaction center by an A–S–D/D″ system with H

The study of the light harvesting and the succeeding charge separation had been performed by photo-electrochemical measurements on the AuOTEs modified with the mixed A–S–D triad monolayer with H (DPyHA, Scheme 4) in our previous work (Fig. 2) [8]. To focus only on the energy transfer process from the pyrene (Py) to the perylene (Pe) moiety, the dependence of sensitized emission inten-

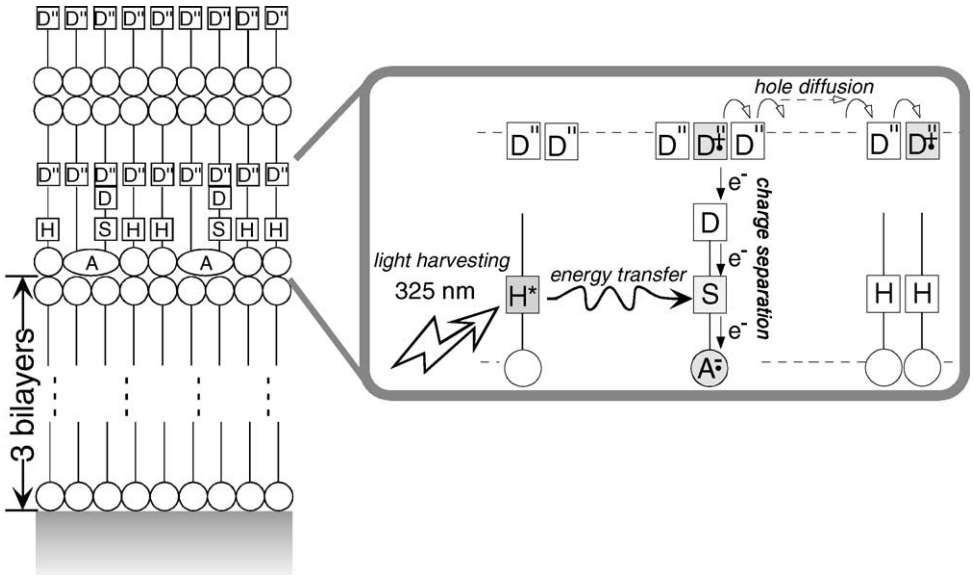

Fig. 18. The schematic illustration of the LB assemblies for simulation of the primary process in natural photosynthetic reaction center. After the deposition of the six monolayers of T, a mixed A–S–D monolayer with H (A–S–D:H = 1:30) and a pure D″ bilayer were deposited. The photo-electric conversion with the LB assemblies is attained by light harvesting, charge separation, and charge diffusion processes.

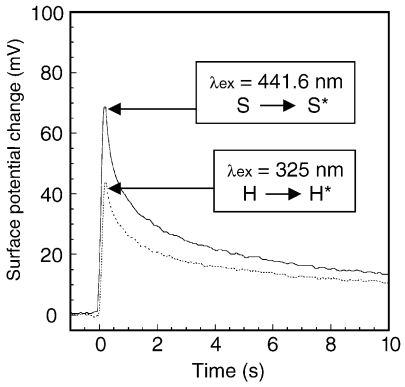

Fig. 19. Photo-induced surface potential change under step illumination by a 441.6 nm (a solid curve) or a 325 nm line (a dotted curve) of a He–Cd laser.

sity on the ratio of H with an energy acceptor molecule had been examined [69]. The result indicates that the most efficient energy transfer from Py* to Pe was attained with the ratio Py:Pe = 30:1.

Based on the energy transfer study, the mixed A–S–D monolayer with H with the molar mixing ratio 1:30 was added by a D″ (Scheme 4) bilayer as shown in Fig. 18. The compound D″ was used as the second donor in this case. Fig. 19 shows the change in surface potential measured with the (A–S–D + H)/D″ system under the step illumination of 441.6 nm (a solid curve) and 325 nm (a dotted curve). With the light illumination at 441.6 nm, the Pe moiety in A–S–D is directly excited and H contributes as a diluent similarly to T in Fig. 17(b), whereas Pe* is induced by energy transfer from Py* of H to Pe under illumination at 325 nm. Although the change in surface potential should not be detectable with such diluted A–S–D layer alone as used in Fig. 15(b), the film added by D″ bilayer gave large surface potential change at both wavelengths. The Py absorbance of the film at 325 nm is estimated to be ca. 25 times larger than that of Pe at 441.6 nm [12,70]. The number of the photons of the incident light at 325 nm is ca. 1/35 against that at 441.6 nm of the He–Cd laser used. Considering the difference between the resulted signals at 325 and 441.6 nm, we could conclude that the light energy harvested by the antenna molecule was mostly funneled to the sensitizer moiety of the A–S–D triad molecule.

6. Conclusions

Principles and characteristics of family members of KFM, SMM, and SSPM and their application to the studies of LB assemblies containing A–S–D triad molecules were described. SMM was found to be used as optical and electronic access tools from the macro-scale external systems to nano-molecular devices.

The charge separation under laser light illumination was observed by SMM on the LB films containing multilayers of alternate triad (or dyad) and inactive fatty acid monolayer. The signs of observed dipole moment changes were in accordance with the directions of charge separation in the unidirectionally oriented triad (or dyad) in the LB films. The slow decays of recombination of the separated charge in the LB films were interpreted in terms of the lateral diffusion of electrons and holes, among the A and the D moieties for the A–S–D triad (or the A and the S moieties for the A–S dyad), respectively. The moderate decrease of the surface concentration of A–S–D (from A–S–D:T = 1:5 to 1:30) caused the abrupt decrease of the change in surface potential. The result supports the assumption of the charge separation mechanism via the lateral charge diffusion.

The effect of addition of the A layer in the order A/A–S–D was significant with the diluted A–S–D layer (A–S–D:T = 1:30). This indicates that the additional A layer has the capability to enhance the electron migration and the electron accumulation. The remarkable increase in the photo-induced surface potential change was observed with A–S–D/D′ structure. The quadruplet structure was found to be essential for efficient charge separations.

Finally, we successfully fabricated the LB assemblies replicating the three aspects of a primary process in natural photosynthesis, i.e. light-harvesting, charge-separation, and charge-diffusion processes.

Acknowledgements

This work was supported by a Grant-in-Aid for Creative Scientific Research on “Devices on molecular and DNA levels” (No. 13GS0017) from the Ministry of Education, Science, Sports, and Culture and by a Grant to M. Sakomura from Foundation Advanced Technology Institute, Japan.

References

[1] A. Ulman, Ultrathin Organic Films, Academic Press, San Diego, CA, 1991.
[2] T. Osa, M. Fujihira, Nature 264 (1976) 349–350.
[3] M. Fujihira, N. Ohishi, T. Osa, Nature 268 (1977) 226–228.
[4] M. Fujihira, in: A.J. Fry, W.E. Britton (Eds.), Topics in Organic Electrochemistry, Plenum, New York, NY, 1986, pp. 255–298.
[5] M. Fujihira, K. Nishiyama, H. Yamada, Thin Solid Films 132 (1985) 77–82.
[6] M. Fujihira, H. Yamada, Thin Solid Films 160 (1988) 125–132.
[7] M. Fujihira, M. Sakomura, Thin Solid Films 179 (1989) 471–476.
[8] M. Fujihira, M. Sakomura, T. Kamei, Thin Solid Films 180 (1989) 43–50.
[9] M. Sakomura, M. Fujihira, Thin Solid Films 243 (1994) 616–619.
[10] M. Sakomura, M. Fujihira, Thin Solid Films 273 (1996) 131–134.
[11] M. Fujihira, Mol. Cryst. Liq. Cryst. 183 (1990) 59–69.
[12] M. Fujihira, M. Sakomura, D. Aoki, A. Koike, Thin Solid Films 273 (1996) 168–176.
[13] M. Fujihira, in: A. Ulman (Ed.), Thin Films, Academic Press, Boston, MA, 1995, pp. 239–277.
[14] M. Fujihira, in: R.R. Birge (Ed.), The Photoinduced Electron Transfer and Energy Transfer in LB Films, American Chemical Society, Washington, DC, Adv. Chem. Ser. 240 (1994) 373–394.

[15] M. Fujihira, in: H.-J. Güntherodt, D. Anselmetti, E. Meyer (Eds.), Forces in Scanning Probe Methods, Kluwer Academic Publishers, Dordrecht, The Netherlands, NATO ASI Ser., Ser. E: Appl. Sci. 286 (1995) 567–591.
[16] M. Sakomura, T. Oono, M. Fujihira, Thin Solid Films 327–329 (1998) 708–711.
[17] M. Sakomura, T. Oono, R. Sakon, M. Fujihira, Ultramicroscopy 91 (2002) 215–220.
[18] J. Deisenhofer, H. Michel, EMBO J. 8 (1989) 2149–2170.
[19] R. van Grondelle, J.P. Dekker, T. Gillbro, V. Sundstrom, Biochim. Biophys. Acta 1187 (1994) 1–65.
[20] M. Fujihira, in: M. Nieto-Vesperinas, N. Garcia (Eds.), Optics at the Nanometer Scale: Imaging and Storing with Photonic Near Fields, Kluwer Academic Publishers, Dordrecht, The Netherlands, NATO ASI Ser., Ser. E: Appl. Sci. 319 (1996) 205–221.
[21] M. Fujihira, in: B. Bhushan (Ed.), Nanotribology, Kluwer Academic Publishers, Dordrecht, The Netherlands, NATO ASI Ser., Ser. E: Appl. Sci. 330 (1997) 239–260.
[22] J. Frommer, Angew. Chem., Int. Ed. 31 (1992) 1298–1328.
[23] R. Overney, E. Meyer, J. Frommer, D. Brodbeck, R. Lüthi, L. Howald, H.-J. Güntherodt, M. Fujihira, H. Takano, Y. Gotoh, Nature 359 (1992) 133–135.
[24] E. Meyer, R. Orverney, R. Lüthi, D. Brodbeck, L. Howald, J. Frommer, H.-J. Güntherodt, O. Wolter, M. Fujihira, H. Takano, Y. Gotoh, Thin Solid Films 220 (1992) 132–137.
[25] G. Binnig, H. Rohrer, C. Gerber, E. Weibel, Phys. Rev. Lett. 49 (1982) 57–61.
[26] G. Binnig, C.F. Quate, C. Gerber, Phys. Rev. Lett. 56 (1986) 930–933.
[27] C.M. Mate, G.M. McClelland, R. Erlandsson, S. Chiang, Phys. Rev. Lett. 59 (1987) 1942–1945.
[28] G. Meyer, N.M. Amer, Appl. Phys. Lett. 57 (1990) 2089–2091.
[29] O. Marti, J. Colchero, J. Mlynek, Nanotechnology 1 (1990) 141–144.
[30] T. Nakagawa, K. Ogawa, T. Kurumizawa, S. Ozaki, Jpn. J. Appl. Phys. 32 (1993) L294–L296.
[31] R. Murry, in: A. Weissberger, W.H. Saunders Jr. (Eds.), Molecular Design of Electrode Surface, Techniques of Chemistry, vol. 22, Wiley, New York, 1992, p. 427.
[32] A. Ulman, Chem. Rev. 96 (1996) 1533–1554.
[33] C.D. Frisbie, L.F. Rozsnyai, A. Noy, M.S. Wrighton, C.M. Lieber, Science 256 (1994) 2071–2074.
[34] A. Noy, C.D. Frisbie, L.F. Rozsnyai, M.S. Wrighton, C.M. Lieber, J. Am. Chem. Soc. 117 (1995) 7943–7951.
[35] A. Noy, C.H. Sanders, D.V. Vezenov, S.S. Wong, C.M. Lieber, Langmuir 14 (1998) 1508–1511.
[36] A. Noy, D.V. Vezenov, C.M. Lieber, Annu. Rev. Mater. Sci. 27 (1997) 381–421.
[37] A. Noy, D.V. Vezenov, L.F. Rozsnyai, C.M. Lieber, J. Am. Chem. Soc. 119 (1997) 2006–2015.
[38] S.S. Wong, E. Joselevich, A.T. Woolley, C.L. Cheung, C.M. Lieber, Nature 394 (1998) 52–55.
[39] S.S. Wong, A.T. Wooley, E. Joselevich, C.L. Cheung, C.M. Lieber, J. Am. Chem. Soc. 120 (1998) 8557–8558.
[40] R. McKendry, M.E. Theoclitou, T. Rayment, C. Abell, Nature 391 (1998) 566–568.
[41] H.X. He, C.Z. Li, J.Q. Song, T. Mu, L. Wang, H.L. Zhang, Z.F. Liu, Mol. Cryst. Liq. Cryst. A 294 (1997) 99–102.
[42] T. Miyatani, M. Horii, A. Rosa, M. Fujihira, O. Marti, Appl. Phys. Lett. 71 (1997) 2632–2634.
[43] T. Miyatani, S. Okamoto, A. Rosa, O. Marti, M. Fujihira, Appl. Phys. A 66 (1998) S349–352.
[44] L. Kelvin, Philos. Mag. 46 (1898) 91–120.
[45] M. Fujihira, Annu. Rev. Mater. Sci. 29 (1999) 353–380.
[46] J.E. Stern, B.D. Terris, H.J. Mamin, D. Ruger, Appl. Phys. Lett. 53 (1988) 2717–2719.
[47] Y. Martin, D.W. Abraham, H.K. Wickramasinghe, Appl. Phys. Lett. 52 (1988) 1103–1105.
[48] M. Nonnenmacher, O. Wolter, J. Greschner, R. Kassing, J. Vac. Sci. Technol. B9 (1991) 1358–1362.
[49] J.M.R. Weaver, H.K. Wickramsinghe, J. Vac. Sci. Technol. B9 (1991) 1562–1565.
[50] J.M.R. Weaver, D.W. Abraham, J. Vac. Sci. Technol. B9 (1991) 1559–1561.
[51] C. Schönenberger, S.F. Alvarado, Phys. Rev. Lett. 65 (1990) 3162–3164.
[52] M. Nonnenmacher, M. O'Boyle, H.K. Wickramsinghe, Appl. Phys. Lett. 58 (1991) 2921–2923.
[53] M. Nonnenmacher, M. O'Boyle, H.K. Wickramsinghe, Ultramicroscopy 42–44 (1992) 268–273.
[54] H. Yokoyama, K. Saito, T. Inoue, Mol. Electron. Bioelectron. 3 (1992) 79–88.
[55] H. Yokoyama, T. Inoue, M. Hattori, K. Saito, in: Proceedings of 11th Symposium on Future Electron Devices, Chiba, 1992, pp. 29–34.
[56] H. Yokoyama, T. Inoue, Thin Solid Films 242 (1994) 33–39.
[57] T. Inoue, H. Yokoyama, Thin Solid Films 243 (1994) 399–402.
[58] T. Inoue, H. Yokoyama, J. Vac. Sci. Technol. B12 (1994) 1569–1571.
[59] M. Fujihira, H. Kawate, M. Yasutake, Chem. Lett. (1992) 2223–2226.
[60] M. Fujihira, H. Kawate, Thin Solid Films 242 (1994) 163–169.
[61] M. Fujihira, H. Kawate, J. Vac. Sci. Technol. B12 (1994) 1604–1608.
[62] M. Fujihira, Ann. N.Y. Acad. Sci. 852 (1998) 306–329.
[63] M. Sakomura, S. Lin, T.A. Moore, A.L. Moore, D. Gust, M. Fujihira, J. Phys. Chem. A 106 (2002) 2218–2226.
[64] T. Watanabe, K. Honda, J. Phys. Chem. 86 (1982) 2617–2619.
[65] J.A. Farrington, M. Ebert, E.J. Land, K. Fletcher, Biochim. Biophys. Acta 314 (1973) 372–381.
[66] M. Sakomura, M. Fujihira, Chem. Lett. (1998) 701–702.
[67] M. Sakomura, M. Fujihira, Thin Solid Films 327–329 (1998) 718–721.
[68] J. Deisenhofer, K. Miki, R. Huber, H. Michel, Nature 318 (1985) 618–624.
[69] M. Fujihira, M. Sakomura, R. Sawada, Mol. Cryst. Liq. Cryst. 322 (1998) 313–318.
[70] M. Fujihira, T. Kamei, M. Sakomura, Y. Tatsu, Y. Kato, Thin Solid Films 179 (1989) 485–492.